Wireless Power Transfer System With an Asymmetric Four-Coil Resonator for Electric Vehicle Battery Chargers

SangCheol Moon, *Member, IEEE*, and Gun-Woo Moon, *Member, IEEE*

***Abstract*—This paper proposes a high-efficiency wireless power transfer system with an asymmetric four-coil resonator. It presents a theoretical analysis, an optimal design method, and experimental results. Multicoil systems which have more than three coils between the primary and secondary side provide the benefits of a good coupling coefficient, a long transfer distance, and a wide operating frequency range. The conventional four-coil system has a symmetric coil configuration. In the primary side, there are source and transmitter coils, and the secondary side contains receiver and load coils. On the other hand, in the proposed asymmetric four-coil system, the primary side consists of a source coil and two transmitter coils which are called intermediate coils, and in the secondary side, a load coil serves as a receiver coil. In the primary side, two intermediate coils boost the apparent coupling coefficient at around the operating frequency. Because of this double boosting effect, the system with an asymmetric four-coil resonator has a higher efficiency than that of the conventional symmetric four-coil system. A prototype of the proposed system with the asymmetric four-coil resonator is implemented and experimented on to verify the validity of the proposed system. The prototype operates at 90 kHz of switching frequency and has 200 mm of the power transmission distance between the primary side and the secondary side. An ac–dc overall system efficiency of 96.56% has been achieved at 3.3 kW of output power.**

***Index Terms*—Battery charger, electric vehicle (EV), multicoil resonator, wireless power transfer (WPT).**

I. Introduction

NOWADAYS, global warming caused by greenhouse gas has become a significant problem in the world. So, the United States (US), the European Union (EU), China, Japan, South Korea, and other countries have proposed and established new fuel economy and car CO2 emission standard which are very challenging when compared with the former regulations.According to the US Environmental Protection Agency, the US is expected to have 58% reduction in CO2 emission by 2025. However, only 5% of vehicles including hybrid electric vehicles (HEV), plug-in hybrid electric vehicles (PHEV), and battery electric vehicles (BEV) made in 2013 could meet CO2 emission target for 2025. Therefore, the automobile industries have been working on the development of HEV, PHEV, and BEV, and they expect EV sales increases to 5.9 million units by 2020. As EV sales increases, the electric vehicle supply equipment (EVSE) market will also increase.

In the EVSE market, a battery charging method can be classified into wired charging and wireless charging. Wired charging uses an ac source on the power outlet by cables and the most current charging stations utilize this method. On the other hand, wireless charging uses induction coils to create an alternating electromagnetic field in the primary side on the floor of the charging station while a second induction coil in the car receives power from the electromagnetic field. The convenience of wireless charging can make EVs more acceptable to drivers because they do not need to handle the power plug which may shock the human body due to very high charging voltage. Wireless charging stations also require less hardware and can be installed underground. Therefore, the wireless power transfer (WPT) technology for EV chargers has been studied and developed for the last few years, and the wireless charging market is expected to grow rapidly.

According to Pike Research, the wireless charging market started slowly by 2013, and it will increase rapidly to 5% of the total revenue by 2017. However, the power transfer efficiency, which is lower than that of the wired ac charging, is a major concern [1]–[6]. Recently, a multicoil resonator which has more than three coils has been studied. Generally, in a multicoil resonator, since the magnetic field is expanded by intermediate coils or relay coils, the coupling between the primary and the secondary side is strengthened. In [7] and [8], power analysis has been carried out to identify the adjacent and nonadjacent power flow components in domino forms. [9] proposed a figure-of-merit to find out whether a two-, three-, or four-coil link is appropriate for their particular application. [10] and [11] investigated a relay or repeater effect to extend the energy transfer distance. [12] and [13] proposed the multicoil array structure which has several identical primary coil in parallel. [14] and [15] analyzed and proposed high efficiency design with an intermediate coil.

The conventional four-coil resonator with a symmetric coil configuration is shown in Fig. 1. In the primary side, there are source and transmitter coils, and the secondary side contains receiver and load coils. In the symmetric coil configuration, the intermediate coils provide an increase of the effective inductances of the source and load coils. However, if the distance between the primary and secondary side is too far, the intermediate coil in the secondary side cannot affect the primary side. Thus,

Manuscript received August 3, 2015; revised October 16, 2015; accepted November 18, 2015. Date of publication December 8, 2015; date of current version May 20, 2016. Recommended for publication by Associate Editor S. Williamson.

S. Moon is with the Analog Power Group, Fairchild Semiconductor, Gyeonggi-do 14487, Korea (e-mail: caprio.moon@fairchildsemi.com).

G.-W. Moon is with the Electrical Engineering, KAIST, Daejeon 305-701, Korea (e-mail: gwmoon@kaist.ac.kr).

Color versions of one or more of the figures in this paper are available online at http://ieeexplore.ieee.org.

Digital Object Identifier 10.1109/TPEL.2015.2506779

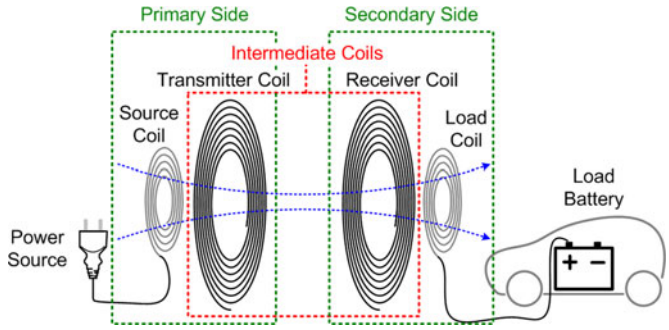

Fig. 1. Conventional symmetric four-coil resonator.

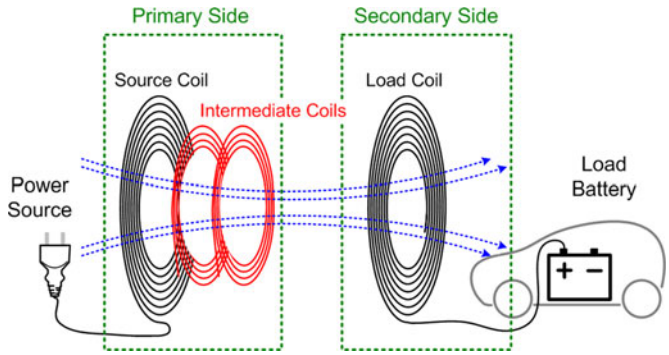

Fig. 2. Proposed asymmetric four-coil resonator.

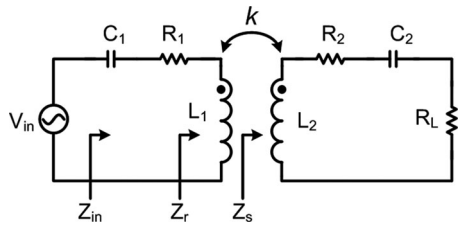

Fig. 3. Equivalent circuit of two-coil resonator system with series-series compensation.

there is only a single boosting effect, which is similar to the three-coil resonator system [14], in the primary side. However, in most WPT systems, the main power losses occur in the primary side because there are many resistive components including inverter switches. Therefore, a reduction of the RMS current in the primary side is an easy way to increase the system efficiency. To achieve a low RMS current in the primary side and a high system efficiency, this paper proposes a WPT system with an asymmetric four-coil resonator as shown in Fig. 2.

II. Analysis of the Proposed Asymmetric Four-Coil Resonator WPT System

When series–series compensation is applied to a two-coil resonator system, the equivalent circuit can be depicted by Fig. 3.

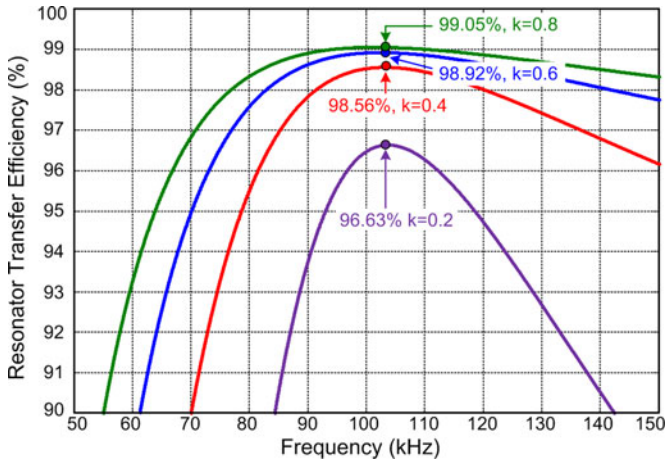

Fig. 4. Transfer efficiency of resonator with various k when, $L_1 = 186.55$ μs, $L_2 = 131.66$ μs, $C_1 = 13.88$ nF, $C_2 = 18.45$ nF, $R_L = 24.24$ Ω.

In this circuit, considering winding resistances R_1 and R_2, the power transfer efficiency η can be calculated by [18], equation (1) as shown at the bottom of the page, where $Z_{\rm in}$, Z_r and Z_s are the input impedance, reflected impedance, and secondary side impedance, respectively. k is the coupling coefficient which is defined as $L_m/(L_{\rm lkp} + L_m)$ between the primary side and the secondary side. R_L is the load resistance. For a high efficiency, the imaginary part of $Z_{\rm in}$ of the system should be removed so that ω is designed by

$$\omega = \omega_0 = \frac{1}{\sqrt{L_1 C_1}} = \frac{1}{\sqrt{L_2 C_2}}. \tag{2}$$

In that case, the transfer efficiency is simplified by

$$\eta = \frac{1}{1 + \frac{R_1(R_2+R_L)}{k^2\omega_0^2 L_1 L_2}} \cdot \frac{R_L}{R_2 + R_L}. \tag{3}$$

This equation shows that η is directly related to k. Thus, a higher k is very important factor for higher efficiency WPT systems. Fig. 4 shows simulation results of the transfer efficiency of the resonator with various k. The higher k can achieve the higher efficiency. In case of $k = 0.4$, the maximum efficiency is increased by 1.93% point compared to $k = 0.2$. But, in case of $k = 0.8$, the maximum efficiency is only increased by 0.13% point compared to $k = 0.6$. It means the efficiency becomes saturate with a coupling coefficient when k is higher than a certain level (e.g., $k = 0.6$). To achieve the higher coupling coefficient, the proposed WPT system utilizes an asymmetric four-coil resonator.

The proposed asymmetric four-coil resonator for WPT systems consists of a source coil and two intermediate coils in the primary side and a load coil in the secondary side as shown in Fig. 5. The source coil and the intermediate coils are placed on

$$\eta = \frac{\mathrm{Re}(Z_r)}{\mathrm{Re}(Z_{\rm in})} \cdot \frac{R_L}{\mathrm{Re}(Z_s)} = \frac{1}{1 + \dfrac{R_1}{(R_2+R_L)k^2 L_1 L_2}\left(\dfrac{(R_2+R_L)^2}{\omega^2} + L_2^2 - \dfrac{2L_2}{\omega^2 C_2} + \dfrac{1}{\omega^4 C_2^2}\right)} \cdot \frac{R_L}{R_2 + R_L} \tag{1}$$

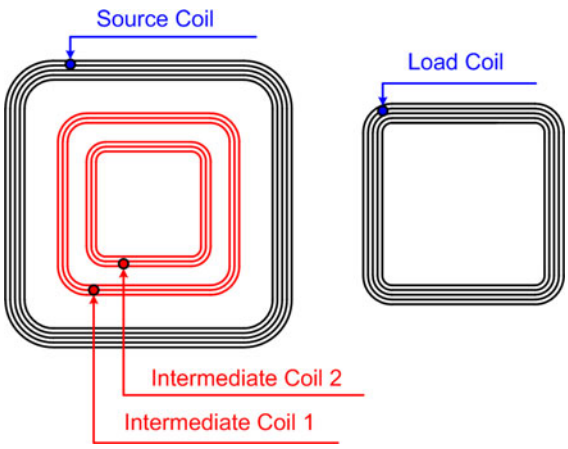

Fig. 5. Configuration of the proposed asymmetric four-coil resonator.

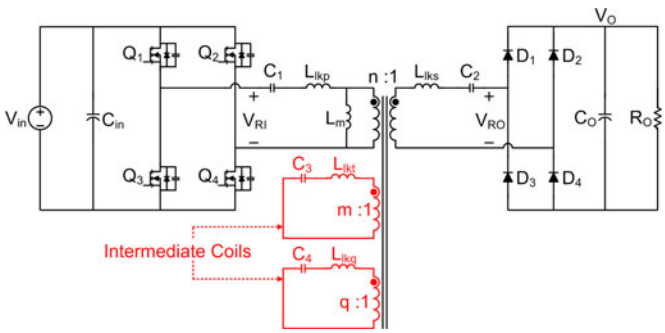

Fig. 6. Equivalent circuit of the proposed asymmetric four-coil system.

a same plane to maximize the power transfer efficiency. Each intermediate coil has resonance capacitor which resonates with the intermediate coil. It is not shown in Fig. 5 for convenience.

In the proposed system, the power transfer efficiency is increased in two ways. First, since each intermediate coil boosts two times, the effective inductance of the source coil in the primary side, the number of turns of the source coil can be reduced so that the equivalent resistance of the coil decreases. Second, because of this double boosting effect, the apparent coupling coefficient at around the switching frequency increases enormously. This higher coupling coefficient makes a circulating current which cannot contribute energy transfer to the load decrease in the primary side so that the RMS input current is reduced.

A. Double Boosting Effect

An equivalent circuit of the proposed asymmetric four-coil system is shown in Fig. 6. A rectified input voltage source $V_{\rm in}$, a full-bridge inverter Q_1–Q_4 for a square wave generator, a resonant capacitor C_1, a source coil, and two intermediate coils are located in the primary side. In the secondary side, there are a load coil, a resonant capacitor C_2, a full-wave rectifier $D_1 - D_4$, and an output load R_o. When the intermediate coils are coupled with the primary coil, as shown in Fig. 6, the physical parameters such as self-inductance and coupling coefficient between the source coil and the load coil are not changed when compared with the two-coil system. However, they boost both the effective

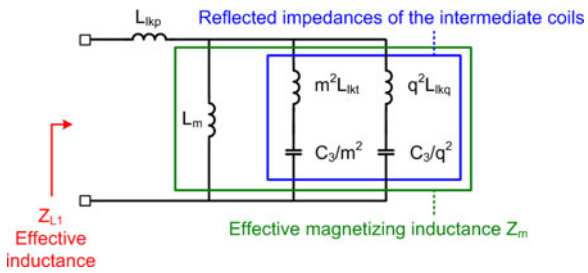

Fig. 7. Equivalent circuit of the effective inductance of the source coil.

self-inductance and magnetizing inductance of the source coil at around the resonance frequencies ω_t and ω_q of the intermediate coils, which are given by

$$\omega_t = \frac{1}{\sqrt{C_3\left(L_{\rm lkt} + \frac{L_m}{m^2}\right)}} \tag{4}$$

$$\omega_q = \frac{1}{\sqrt{C_4\left(L_{\rm lkq} + \frac{L_m}{q^2}\right)}} \tag{5}$$

where $L_{\rm lkt}$ and $L_{\rm lkq}$ are the leakage inductances of the intermediate coils, m and q are the turns ratios between the source coil and intermediate coils, and C_3 and C_4 are the resonance capacitances of the intermediate coils. These intermediate coils induce an increase of the apparent coupling coefficient k_a between the source coil and the load coil. As a result, the power transfer efficiency of the proposed asymmetric four-coil resonator is increased.

When the load coil in Fig. 6 is open-circuited, the equivalent circuit for Z_{L1} of the source coil can be depicted as Fig. 7. Since two intermediate coils can be reflected to the primary side, Z_{L1} of the source coil is represented by total impedance which has a 90° phase angle as follows:

$$\begin{aligned} Z_{L1} &= |sL_{\rm lkp} + Z_m| \\ &= \left| sL_{\rm lkp} + \frac{sL_m\left(s^2L_{\rm lkt}C_3+1\right)\left(s^2L_{\rm lkq}C_4+1\right)}{\left(s^2\left(m^2L_{\rm lkt}+L_m\right)\frac{C_3}{m^2}+1\right)\left(s^2L_{\rm lkq}C_4+1\right)+\left(s^2L_{\rm lkt}C_3+1\right)s^2L_m\frac{C_4}{q^2}} \right|. \end{aligned} \tag{6}$$

In the case of the single boosting system, when $L_{\rm lkq}$ and C_4 are open-circuited, (6) becomes

$$Z_{L1.\rm single} = \left| sL_{\rm lkp} + \frac{sL_m\left(s^2L_{\rm lkt}C_3+1\right)}{\left(s^2\left(m^2L_{\rm lkt}+L_m\right)\frac{C_3}{m^2}+1\right)} \right|. \tag{7}$$

If the operating frequency f_s is designed as

$$f_s < 1/\left(2\pi\sqrt{L_{\rm lkt}C_3}\right). \tag{8}$$

The denominator of (6) is deceased by $s^2L_mC_4/q^2$. Thus, Z_{L1} of the double boosting system becomes higher than that of the single boosting system.

In the proposed system, the apparent coupling coefficient k_a between the source coil and the load coil can be defined by

$$k_a = \frac{Z_m}{|sL_{\rm lkp} + Z_m|} = \frac{Z_m}{Z_{L1}}. \tag{9}$$

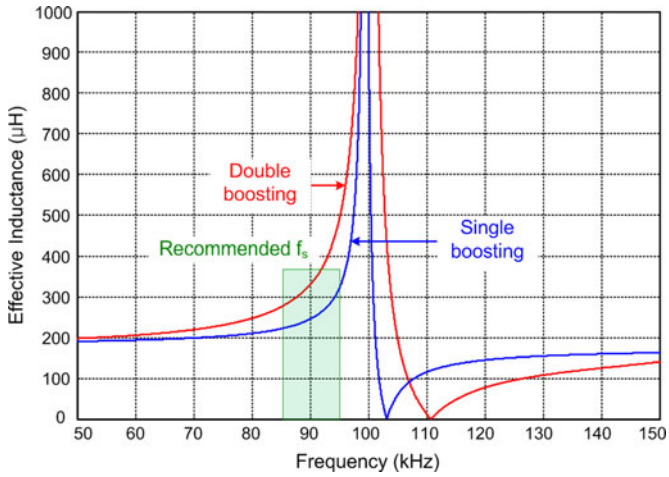

Fig. 8. Effective inductance graphs in cases of single and double boosting systems.

In the proposed resonator, Z_{L1} is measured at the ends of the source coil when the load coil is open-circuited which means C_2 is disconnected, and two intermediate coils are closed-circuited with C_3 and C_4. The load coil short-circuited inductance Z_{LS} is also measured at the ends of the source coil when the load coil is short-circuited, and two intermediate coils are still closed-circuited with C_3 and C_4. Assuming $L_{\rm lkp} = n^2 L_{\rm lks}$, Z_{LS} in given by

$$Z_{LS} = |sL_{\rm lkp} + Z_m || sL_{\rm lkp}|\,. \tag{10}$$

Thus, using (6) and (10), Z_m can be expressed by

$$Z_m = \sqrt{Z_{L1}^2 - Z_{L1} Z_{LS}}. \tag{11}$$

Fig. 8 shows effective inductance graphs which have the single boosting effect of the conventional system and the double boosting effect of the proposed system, respectively. In case of the single boosting system, $Z_{L1.\rm single}$ increases very rapidly. On the other hand, in the double boosting system, Z_{L1} is increased slowly and it is higher than that of the single boosting system because Z_{L1} is boosted two times by each of the intermediate coils at around their *LC* resonance frequencies ω_t and ω_q. Therefore, the proposed system has a higher $k_{\rm a}$ than that of the conventional single boosting system so that the power transfer efficiency is increased. If a WPT system operates in the right side having a steep slope in the recommended range, the effective inductance may vary rapidly with frequency variations of the control IC. As a result, the systems may be unstable and the output voltage may have severe fluctuations. Therefore, the operating frequency should be determined to have a low slope as the recommended operating frequency range.

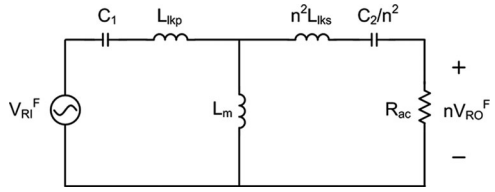

Fig. 9. AC equivalent circuit of two-coil system.

B. Voltage Conversion Ratio

Since most multicoil systems are derived from the conventional two-coil system which has four compensation topologies [16]–[18], the voltage conversion ratio of the proposed system can also be derived from the conventional two-coil system. Considering the conventional two-coil system, which is the same as Fig. 6 except for the intermediate coils, the ac equivalent circuit of the two-coil system with ac load resistance R_{ac} can be illustrated in Fig. 9. To simplify the analysis, only the fundamental components of the resonator input voltage V_{RI} and output voltages V_{RO} are considered to derive the voltage conversion ratio. From the ac equivalent circuit, the input to output voltage conversion ratio T_v is shown in (12), at the bottom of this page. When the resonance frequency of the load coil is tuned at the resonance frequency of the source coil as shown in (2) to maximize the transfer efficiency of the resonator, (12) is rearranged as (13). The denominator of (13) shows that the two-coil resonator system has three resonance frequencies, ω_1, ω_2, and ω_3, as follows:

$$\omega_1 = \frac{1}{\sqrt{C_1(2L_m + L_{\rm lkp})}} \tag{14}$$

$$\omega_2 = \frac{1}{\sqrt{C_1 L_{\rm lkp}}} \tag{15}$$

$$\omega_3 = \frac{1}{\sqrt{C_1(L_m + L_{\rm lkp})}}. \tag{16}$$

ω_1 and ω_2 have voltage follower characteristics that make the real part zero, and the other frequency, which is normally selected as an operating frequency, makes the imaginary part zero of the denominator of (13).

$$T_v = \frac{n \cdot V_o}{V_{\rm in}} = \left| \frac{R_{ac} s^3 C_1 \frac{C_2}{n^2} L_m}{R_{ac} \cdot \frac{sC_2}{n^2} \cdot \left(1 + s^2 C_1 (L_m + L_{\rm lkp})\right) + s^4 C_1 \frac{C_2}{n^2} (n^2 L_{\rm lks} L_m + n^2 L_{\rm lks} L_{\rm lkp} + L_{\rm lkp} L_m) + s^2 C_1 (L_m + L_{\rm lkp}) + s^2 \frac{C_2}{n^2} (n^2 L_{\rm lks} + L_m) + 1} \right| \tag{12}$$

$$T_v = \frac{n \cdot V_o}{V_{\rm in}}\bigg|_{\sqrt{L_1 C_1} = \sqrt{L_2 C_2}} = \left| \frac{R_{ac} s^3 C_1 \frac{C_2}{n^2} L_m}{R_{ac} \cdot \frac{sC_2}{n^2} \cdot \left(1 + s^2 C_1 (L_m + L_{\rm lkp})\right) + (1 + s^2 C_1 L_{\rm lkp})(1 + s^2 C_1 (2L_m + L_{\rm lkp}))} \right| \tag{13}$$

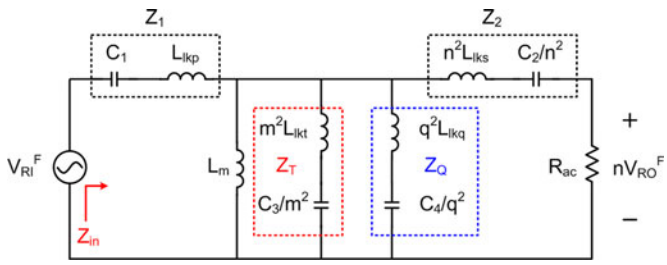

Fig. 10. AC equivalent circuit of the proposed four-coil system.

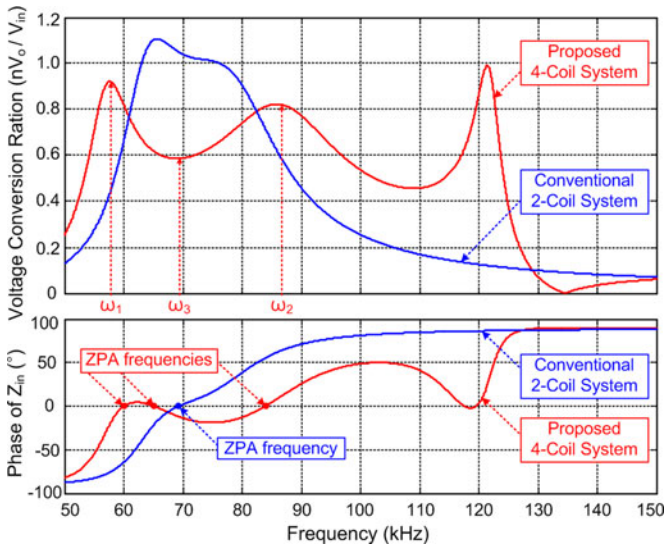

Fig. 11. Comparison of $V_o/V_{\rm in}$ and the phase of $Z_{\rm in}$ between the proposed four-coil system and the conventional two-coil system, when $L_{\rm lkp} = 116.50$ μH, $L_m = 69.83$ μH, $L_{\rm lks} = 76.83$ μH, $L_{\rm lkt} = 20.06$ μH, $L_{\rm lkq} = 15.80$ μH, $C_1 = 28.2$ nF, $C_2 = 42.73$ nF, $C_3 = 69.71$ nF, $C_4 = 47.21$ nF, $n = 1.2315$, $m = 2.4098$, $q = 2.7157$, and $R_o = 24.24$ Ω.

In the proposed four-coil system, the reflected impedances Z_T and Z_Q of the intermediate coils are added parallel to the magnetizing inductance of the conventional two-coil system as shown in Fig. 10. Thus, the voltage conversion ratio $T_{v.4\rm coil}$ is easily derived from (13)

$$T_{v.4\rm coil} = \frac{n \cdot V_o}{V_{\rm in}} = T_v \cdot \overbrace{\left| \frac{Z_T || Z_Q}{Z_T || Z_Q + Z_1 || sL_m || (Z_2 + R_{ac})} \right|}^{\rm Intermediate\ coils\ effect}. \tag{17}$$

Since (17) involves the term T_v, the proposed four-coil system shows similar characteristic at around ω_1, ω_2, and ω_3. However, they are not exactly the same location because of the intermediate coil effect. Both the voltage conversion ratio and the phase of $Z_{\rm in}$ of the proposed four-coil system and the conventional two-coil system are compared in Fig. 11 with practical parameters. Since the intermediate coil effect in the proposed four-coil system increases the apparent coupling coefficient, the bi-furcation phenomenon [19] which has double peaks at ω_1 and ω_2 occurs. As a result, the zero phase angle (ZPA) frequency which shows a high-power transfer efficiency becomes three points at around ω_1, ω_2 and ω_3. Theoretically, the conventional two-coil system can have similar three ZPA frequencies. However, in this case, there is just one ZPA frequency at around ω_3 due to low coupling. In terms of voltage conversion ratio, it may increase or decrease according to the phase of the intermediate coils effect when compared to the conventional one.

III. Design Considerations and Misalignment Tolerance

A. Design Considerations

When the specifications of a WPT system are given as follows, the design parameters such as f_s, f_3, n, R_{ac}, C_1, L_1, C_2, L_2, C_3, L_3, C_4, and L_4 need to be determine properly:

1) power supply : three phase ac source;
2) nominal $V_{\rm in}$: 550 $V_{\rm DC}$ (output of the PFC stage);
3) rated output : $P_o = 6.6$ kW, $V_o = 400$ $V_{\rm DC}$, $I_o = 16.5$ A, and $R_o = 24.24$ Ω;
4) estimated overall system efficiency: $\eta_{\rm est} = 90\%$.

First, the operating frequency f_s of the full-bridge inverter is determined by the recommended range of the switching devices. When silicon MOSFETs are utilized for the inverter, the range of 50–150 kHz frequency is recommended. Furthermore, in order to make the system design easy, f_s is set to be equal to f_2 of (15) which has the voltage follower characteristic. In most WPT systems, f_s is designed to be equal to f_3 of (16) to maximize the transfer efficiency. However, the proposed system has a very high k_a due to intermediate coil effect so that the bifurcation phenomenon occurs. This induces a ZPA frequency at around f_2. Thus, the design which sets f_s equal f_2 has the advantages of a high-power transfer efficiency and the voltage follower characteristic. These provide convenience in terms of the WPT system design.

Second, since typical WPT systems have a weak coupling coefficient of about 0.2–0.3, the impedance matching frequency f_3 between the source coil and the load coil is determined to be 10–20% below f_s. By this assumption, the range of f_3 is calculated by

$$0.83 f_s|_{k=0.3} < f_3 < 0.89 f_s|_{k=0.2}. \tag{18}$$

The third step is determining an effective turns ratio *n* which is a self-inductance square root ratio of the source and load coils, and the ac equivalent load resistance R_{ac}. For an ideal case, $nV_o/V_{\rm in}$ of (13) is unity at f_2. However, considering the system efficiency $\eta_{\rm est}$, the turns ratio is given by

$$n = \eta_{\rm est} \cdot V_{\rm in}/V_o|_{f=f_2} \tag{19}$$

where *n* may be different from the ratio of the physical number of turns, when there is diameter difference between the source and load coils. The ac equivalent load resistance [20] under the rated load condition can be calculated by

$$R_{\rm ac} = \frac{8n^2}{\pi^2} \cdot R_o. \tag{20}$$

The next step is the design of the self-inductances L_1 and L_2 which are measured with the other coils open-circuited, and the resonance capacitances C_1 and C_2 in Fig. 12. C_1 is determined

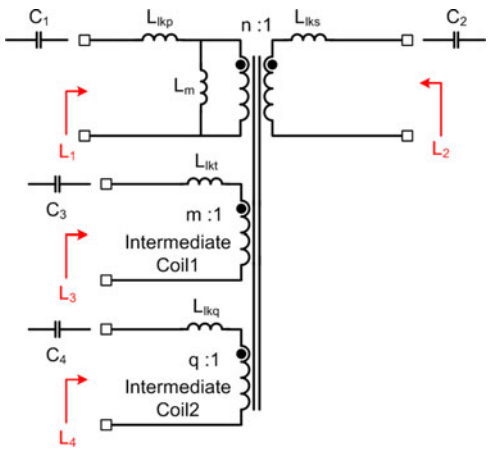

Fig. 12. Design parameters of a resonator.

by the voltage conversion ratio at ω_3 as follows:

$$T_v = \frac{nV_o}{V_{\text{in}}}\bigg|_{\omega=\omega_3} = \left|\frac{R_{\text{ac}}\cdot\omega_3 C_1}{1-\omega_3^2 C_1 L_{\text{lkp}}}\right| = \left|\frac{R_{\text{ac}}\cdot\omega_3 C_1}{k}\right|. \quad (21)$$

Experimentally, T_v is recommended to be around 1.5 to have a low RMS current in the primary side. L_1 and L_2 are given by (16) and $L_2 = L_1/n^2$, respectively. C_2 is determined by impedance matching between the source coil and the load coil as follows:

$$\omega_3 = \omega_{L1C1} = \omega_{L2C2} = \frac{1}{\sqrt{L_1 C_1}} = \frac{1}{\sqrt{L_2 C_2}}. \quad (22)$$

The final step is the design of the intermediate coil resonance components L_3, L_4, C_3, and C_4. When the proposed asymmetric four-coil system is configured as shown in Fig. 5, L_3 and L_4 are designed to make the quality factor of the intermediate coils Q_{in1} and Q_{in2} about 500–600 to minimize the conduction losses of the intermediate coils

$$L_3 = \frac{Q_{\text{in1}} r_{\text{in1}}}{\omega_s} \quad (23)$$

$$L_4 = \frac{Q_{\text{in2}} r_{\text{in2}}}{\omega_s} \quad (24)$$

where r_{in1} and r_{in2} are the ac resistances of intermediate coil1 and coil2, respectively. In the design of C_3, the resonance frequency of intermediate coil1 can be determined by placing it about 15–20% above f_s as follows:

$$\omega_{L3C3} = 1.18\omega_s \quad (25)$$

$$C_3 = \frac{1}{L_3(1.18\omega_s)^2}. \quad (26)$$

Similarly, C_4 is designed to have the resonance frequency f_{L4C4} that is 30–40% above f_{L3C3}

$$C_4 = \frac{1}{L_4(1.35\omega_{L3C3})^2}. \quad (27)$$

If f_{L4C4} is too close to f_{L3C3}, the WPT system may operate in the right side of the recommended range in Fig. 8. Therefore, it is important to maintain a proper frequency distance between f_{L3C3} and f_{L4C4} in the proposed design method. The design

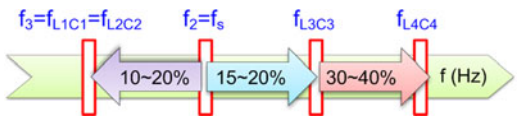

Fig. 13. Design guideline of resonance frequencies.

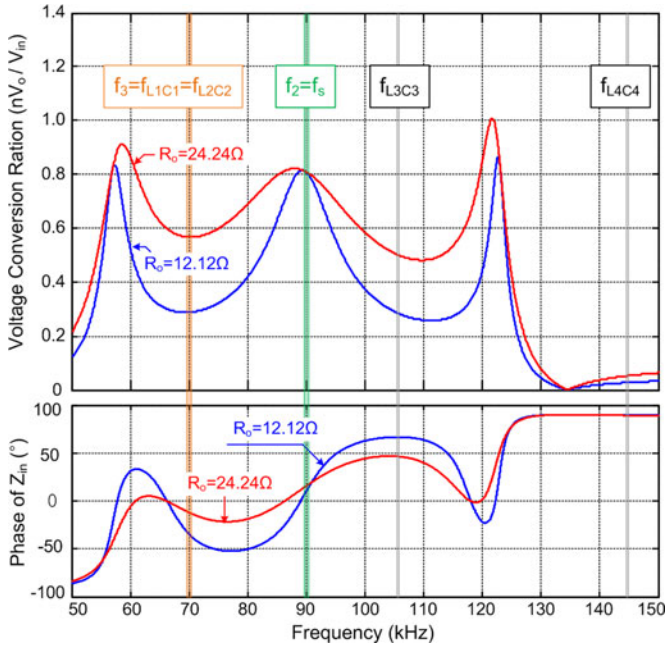

Fig. 14. Design verification using simulation result.

guideline of the resonance frequencies for all of the coils is illustrated and summarized in Fig. 13. Finally, in Fig. 14, the voltage conversion ratio and the phase of Z_{in} for the overall system designed by the guideline are simulated. From this result, it is verified that the system can operate in the ZVS region at f_s with load variations.

B. Misalignment Tolerance

In order to achieve a high-power transfer efficiency, perfect alignment between the source coil and the load coil is very important. This is because the flux density tends to be concentrated at the center of the source coil and the load coil [21]. However, in practice, the source coil and the load coil are usually misaligned. As a result, lateral, vertical and angular misalignments have been analyzed and examined in several studies [21]–[25]. In recent studies, [26]–[31] a resonator structure and a control method which show strong misalignment tolerance have been proposed.

In this section, the performance of the proposed WPT system is investigated when the load coil is misaligned from the source coil as shown in Fig. 15. In EV applications, it is difficult to ensure perfect alignment between the source coil and the load coil. For example, improper parking can induce lateral misalignment during battery charging. In addition, the height from the floor where the source coil is located to the EV body which houses the load coil varies depending on the motor company and vehicle model. These two kinds of misalignment can make the coupling

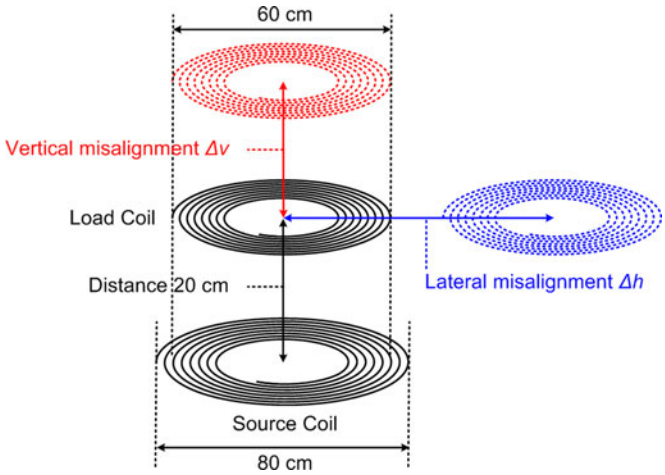

Fig. 15. Lateral and vertical misalignments configuration between the source coil and load coil.

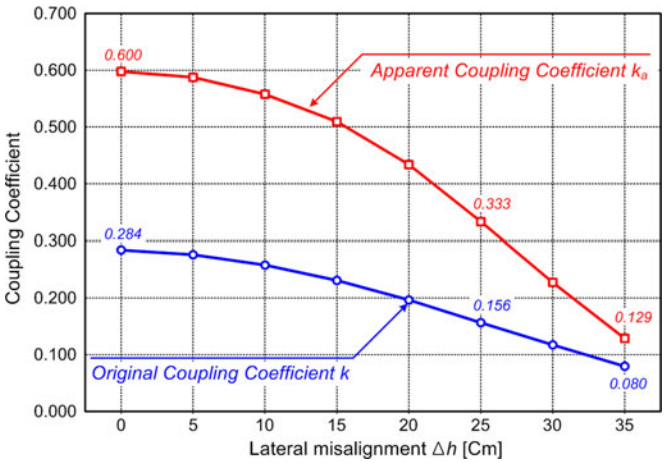

Fig. 16. Measured coupling coefficient with lateral misalignment of the proposed asymmetric four-coil resonator.

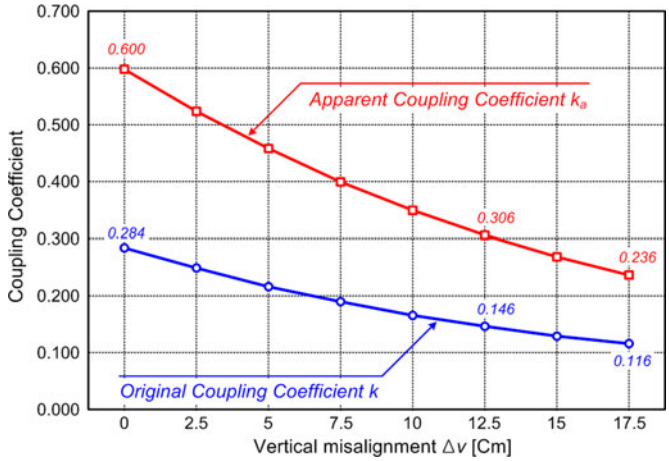

Fig. 17. Measured coupling coefficient with vertical misalignment of the proposed asymmetric four-coil resonator.

TABLE I
SPECIFICATIONS OF PROTOTYPE

3Φ line voltage $V_{\rm line}$ (line-line)	337.5 Vac
Rated output voltage V_o	283 Vdc
Rated output load current I_o	11.66 A
Rated load resistance R_o	24.24 Ω
Rated output power P_o	3.3 kW
Switching frequency f_s	90 kHz
Inverter switches Si MOS.(Q_1, Q_2, Q_3, Q_4)	FCH041N60F (Fairchild Semiconductor)
Output rectifier diodes (D_1, D_2, D_3, D_4)	RURG8060 (Fairchild Semiconductor)
Design Parameters	Values
Self-inductance L_1	186.33 μH
Self-inductance L_2	122.87 μH
Self-inductance L_3	32.09 μH
Self-inductance L_4	25.27 μH
Resonance Capacitance C_1	28.20 nF (EACO)
Resonance Capacitance C_2	42.73 nF (EACO)
Resonance Capacitance C_3	69.71 nF (EACO)
Resonance Capacitance C_4	47.21 nF (EACO)
Original coupling coefficient k	0.284
Apparent coupling coefficient k_a @ 90 kHz	0.600
Turns ratio n	1.2315
Turns ratio m	2.4098
Turns ratio q	2.7157

rate weak as shown in Figs. 16 and 17, and lead the full-bridge inverter in the primary side to nonoptimum switching operation, which will degrade the power transfer efficiency.

Fig. 16 shows the original coupling coefficient k of the two-coil resonator without intermediate coil and the apparent coupling coefficient k_a of the proposed asymmetric four-coil resonator at the operating frequency according to a lateral misalignment Δh from 0 to 35 cm. Through the graph, it can be easily seen that k and k_a decrease with an increase in the lateral misalignment. In the case of k_a, it approaches k with increasing Δh because the intermediate coil effect disappears as Δh increases. In the lateral misalignment range, k_a until 25 cm of Δh is higher than k at perfect alignment. Since coupling coefficient is strongly related with the system efficiency, it is estimated that the system efficiency of the proposed system at 25 cm of Δh is similar with that of the two-coil system at perfect alignment. If misalignment tolerance is defined that the distance from perfect alignment of the two-coil system to Δh of the proposed system which shows similar efficiency, the proposed system has about 25 cm of lateral misalignment tolerance.

In case of vertical misalignment Δv, as shown in Fig. 17, k and k_a also decrease with an increase in Δv. However, unlike the case of the lateral misalignment, since the two intermediate coils still affect k_a regardless of Δv, k_a becomes almost twice k. In the vertical misalignment range, it can be seen from Fig. 17 that the proposed system has about 12.5 cm of vertical misalignment tolerance. This means the proposed system with 32.5 cm of the transmission distance between the source coil and the load coil shows similar efficiency with the two-coil system with 20 cm of the distance.

IV. EXPERIMENTAL RESULTS

A prototype of a 3.3-kW WPT system which has a distance between the primary and the secondary side of 200 mm is implemented with the proposed asymmetric four-coil resonator and the specifications shown in Table I. The prototype operates at 90 kHz of switching frequency and FCH041N60F MOSFETs are

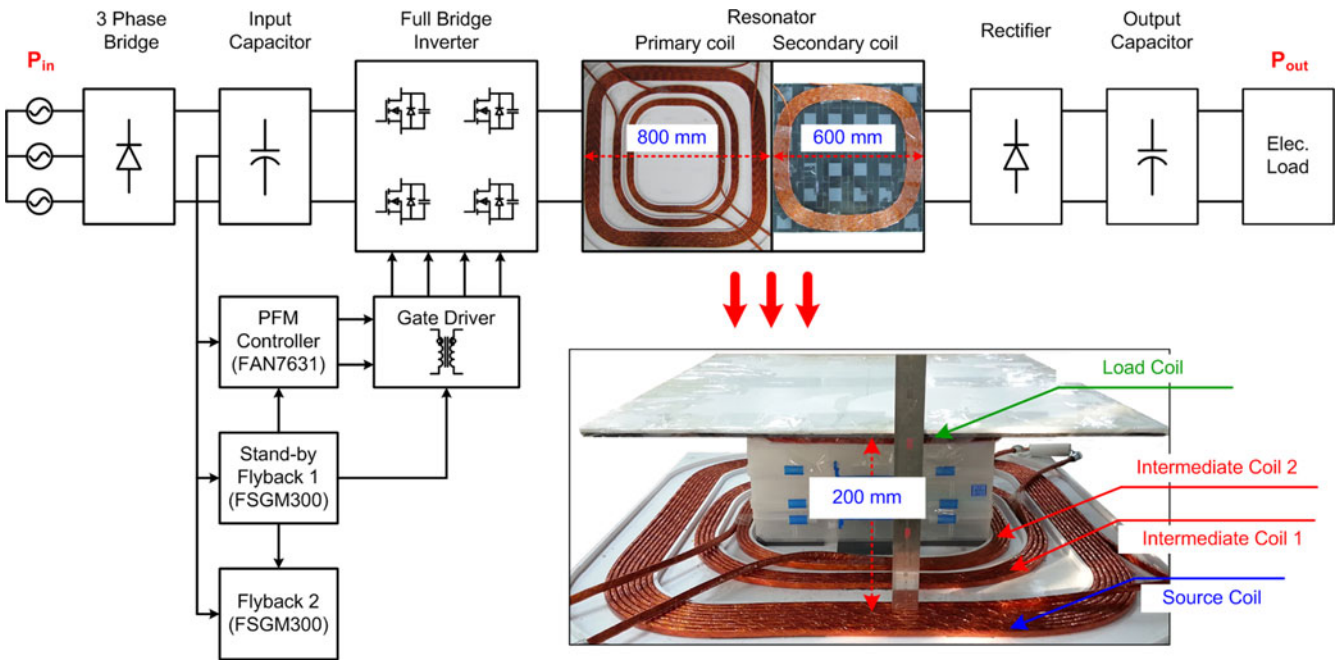

Fig. 18. Block diagram of the proposed asymmetric four-coil system.

used for the full-bridge inverter. The design parameters, which are provided in Section III-A, are measured after the construction of the proposed asymmetric four-coil resonator. In terms of the coupling coefficient, the original coupling coefficient k was measured at 0.284 with the intermediate coils open-circuited. However, after they are turned to closed circuits by connecting resonator capacitors C_3 and C_4 to the intermediate coils, the apparent coupling coefficient k_a is increased by 0.600 at the operating frequency of 90 kHz. Therefore, the proposed system is considered to be a strong coupled system which shows a higher power transfer efficiency than that of a weak coupled system.

Fig. 18 shows a block diagram of the proposed asymmetric four-coil system. From the three-phase ac source, the power is transferred through the full-bridge inverter, the resonator, the output rectifier, and the load. To verify the efficiency of the proposed system only, three-phase power factor correction circuit is not applied. In the resonator, the ratio of transmission distance and the radius of the source coil is about 1/2 so that this system can be considered near-field transmission system. The intermediate coils are constructed as shown in Fig. 5. Innermost winding is intermediate coil2, which has an inductance L_4 of 25.27 μH and is connected to a capacitor C_4 of 47.21 nF. Intermediate coil1 is located between intermediate coil2 and the source coil. The inductance of intermediate coil1 is 32.09 μH and the resonance capacitance C_3 is 69.71 nF. The resonance frequencies f_{L3C3} and f_{L4C4} of intermediate coil1 and coil2 are 106.4 and 145.7 kHz, respectively. Stand-by flyback converters supply the operating current of the PFM controller and the gate drivers.

Experimental current waveforms under the 3.3-kW output load condition are shown in Fig. 19. In these waveforms, the current of the source coil is yellow color, the current of the load coil is colored by green, and the currents of intermediate coil1 and coil2 are blue and red color, respectively. As shown in Fig. 19(a), the proposed system shows peak source current of 12.2 A in the primary side. Though 22.1-A peak current flows through intermediate coil1, the conduction loss is only about 6 W due to low winding resistance of 26 mΩ. Fig. 19(b) shows current waveforms of the single boosting system. The source coil has the same design with that of the proposed four-coil system. The intermediate coil has an inductance of 49.83 μH and capacitance of 41.21 nF. The resonant capacitances of the source coil and load coil are 19.43 and 25.08 nF, respectively. The operating frequency is designed by 100 kHz and k_a is measured by 0.408. In this case, the peak source current is slightly increased to 14.2 A. It results in increase of the conduction loss in the primary side when compared with the proposed system. Fig. 19(c) shows the conventional two-coil system. The source coil is also the same with that of the proposed system. The resonant capacitances of the source coil and load coil are 13.88 and 18.45 nF, respectively. Thereby, the resonant frequency of the primary side and the secondary side are 98.9 and 102.1 kHz, respectively. Though, perfect matching between the resonant frequencies of the primary side and the secondary side can increase the system efficiency more, that work is very difficult due to discrete capacitance and its tolerance. In the configured two-coil system, the coupling coefficient is 0.191 and the operating frequency is 97 kHz. The peak source current highly increases to 23 A due to low coupling coefficient. It results in high conduction loss in the primary side. After all, the intermediate coil effect is tradeoff between the source coil current and the intermediate coils current. If the intermediate coil is utilized, the current of the source coil decreases and the current of the intermediate coil increases. Since the source coil current flows

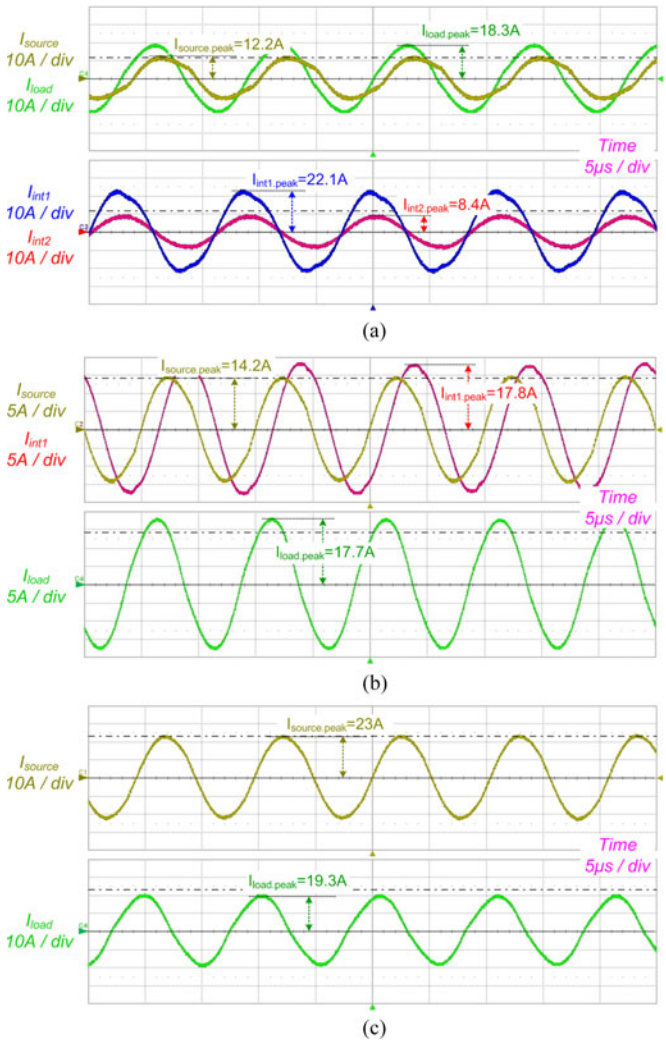

Fig. 19. Current waveforms at 3.3-kW output power (a) the proposed asymmetric four-coil system (b) the single boosting system (c) the conventional two-coil system.

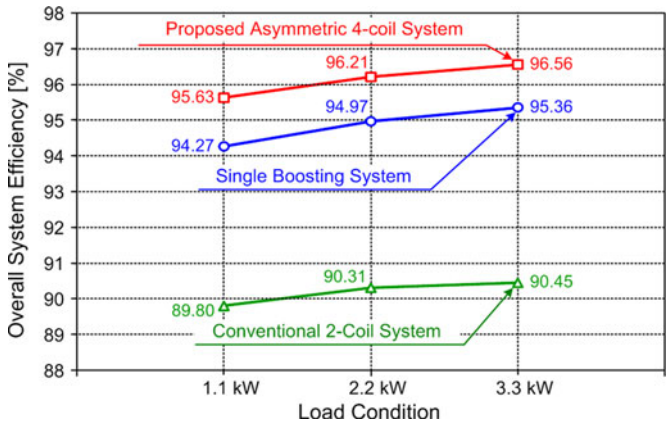

Fig. 20. Overall system efficiency with load variation.

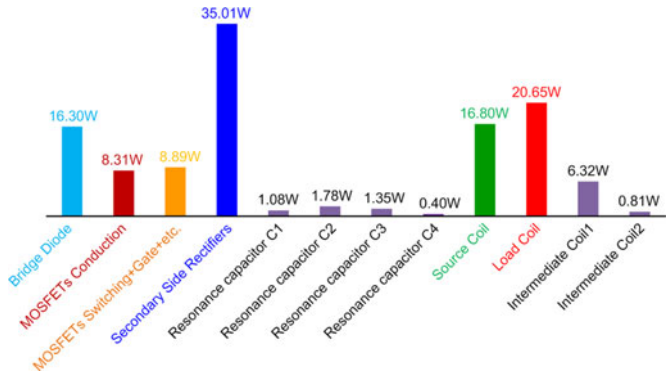

Fig. 21. Loss analysis of the proposed system.

through the whole primary side components such as full-bridge inverter, lower source coil current is very effective to increase the system efficiency.

Fig. 20 shows the overall system efficiency with load variations for the proposed asymmetric four-coil system, the single boosting system which has an intermediate coil [14], and the conventional two-coil system. Since the proposed system has a higher apparent coupling coefficient caused by double boosting, the proposed system shows a 96.56% overall system efficiency from the three phase ac source to the output load. It is about 1.2% point higher than the single boosting system which has a k_a of 0.408 in a wide load range. In the conventional two-coil system, since there is no boosting effect, the system has very low k of 0.191 so that the efficiency is about 5% point lower than that of the proposed system. These efficiency differences are also verified by the simulation result of the resonator transfer efficiency as shown in Fig. 4. When the coupling coefficient is increased from 0.2 to 0.4, the transfer efficiency is significantly increased. It corresponds to the experimental results of the conventional two-coil system and the single boosting system. In case of increase of k from 0.4 to 0.6, the efficiency improvement is still acceptable. It is similar with the efficiency improvement of the proposed system. But, in the simulation result, higher k than 0.6 cannot provide sufficient increase of the efficiency. This means intermediate coils more than three cannot provide sufficient benefit in the efficiency point of view. In the proposed system, there is still a chance to increase the efficiency in terms of the secondary side rectifiers by replacing the diode rectifiers with synchronous rectifiers.

Under the 3.3-kW output load, the total losses of the proposed system and the single boosting system are analyzed in Figs. 21 and 22, respectively. In the secondary side, the proposed system and the single boosting system show similar losses of the secondary side rectifiers and the load coil. However, in the primary side, losses of the MOSFETs conduction and the source coil have half the losses of the single boosting system because of the low circulating current caused by a higher k_a. These result in an efficiency improvement when compared to the single boosting system.

Fig. 23 shows the overall system efficiency with lateral and vertical misalignments at 1 kW of output power. To regulate 1-kW output power, the input voltage of the full-bridge inverter was controlled. As mentioned in Section III-B, in terms of lateral misalignment, the proposed system has about 25 cm of

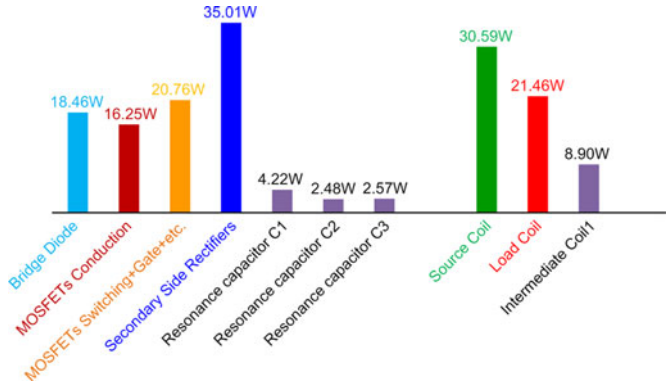

Fig. 22. Loss analysis of the single boosting system.

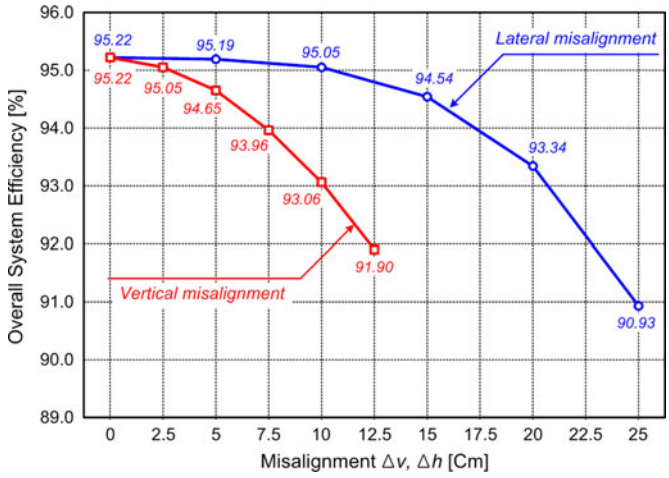

Fig. 23. Overall system efficiency with lateral and vertical misalignments.

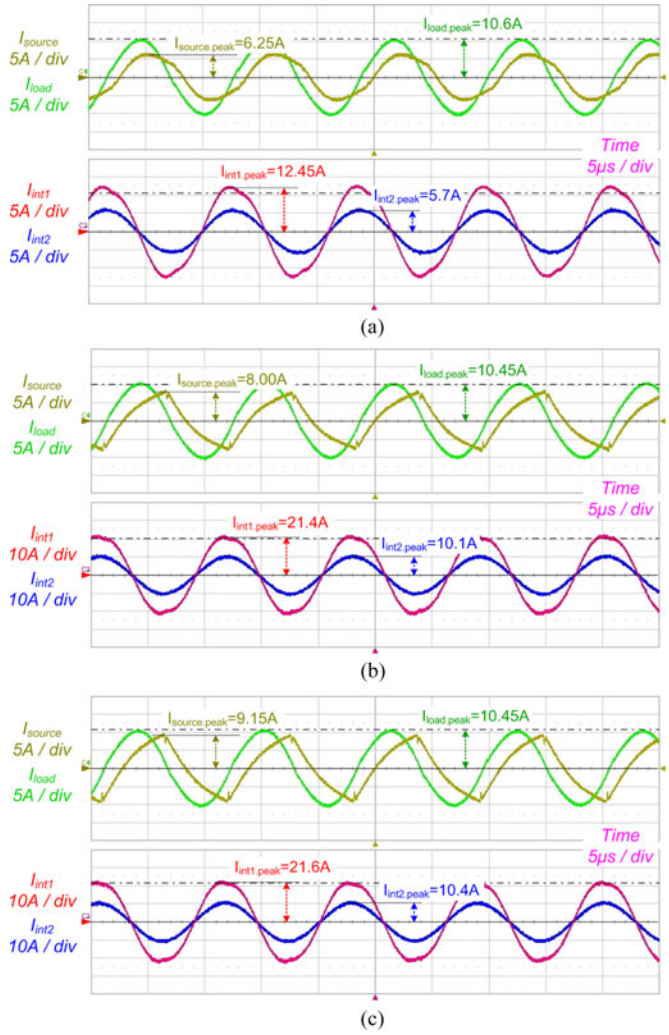

Fig. 24. Current waveforms under misalignment conditions (a) the perfect alignment condition (b) Lateral misalignment of 20 cm (c) Vertical misalignment of 10 cm.

misalignment tolerance, and the efficiency is higher than 90% at 25 cm. In the case of vertical misalignment, the efficiency is around 91.90% at 12.5 cm vertical misalignment which is totally 32.5 cm of power transmission distance. On the other hand, the conventional two-coil system in Fig. 20 shows about 90% efficiency with perfect alignment condition. Although the proposed system has no special control method for the misalignment, the system shows wide misalignment tolerance.

The current waveforms of the proposed system under misalignment conditions are shown in Fig. 24. First, in the perfect alignment condition, the current waveforms are shown in Fig. 24(a). The lateral misalignment of 20 cm and the vertical misalignment of 10 cm are also shown in Fig. 24(b) and (c), respectively. Though these misalignments do not lead the inverter MOSFETs to hard switching operation, the source currents increase about 30% point – 40% point. In particular, the currents of the intermediate coils are increased about 100% point. These current levels are similar with the currents of 3.3-kW condition with the perfect alignment as shown in Fig. 19(a). The results mean huge circulating current flows in the primary side under misalignment. Therefore, thermal problem may occur in these conditions.

V. Conclusion

In this paper, a WPT system with an asymmetric four-coil resonator for electric vehicle battery chargers has been proposed. In the proposed system, two intermediate coils in the primary side boost two-times the effective inductance of the source coil at around their *LC* resonance frequencies. As a result, the apparent coupling coefficient at the operating frequency is enhanced much more than that of the single boosting system. Thus, the proposed system can reduce the number of turns in the source coil and the RMS input current when compared to the single boosting system and the conventional two-coil system. As a result, the proposed system has a higher power transfer efficiency with a relatively long distance between the source coil and load coil. To verify the proposed asymmetric four-coil resonator WPT system, a 3.3-kW prototype was implemented and experimented on. The results showed that the proposed WPT system has an very high ac–dc overall efficiency of 96.56% with a 200 mm of power transmission distance under a 3.3-kW output load condition, and wide lateral and vertical misalignment

tolerances. Therefore, the proposed system can be a good candidate for the electric vehicle wireless charger.

REFERENCES

[1] J. Deng, W. Li, T. D. Nguyen, S. Li, and C. C. Mi, "Compact and efficient bipolar coupler for wireless power chargers: Design and analysis," *IEEE Trans. Power Electron.*, vol. 30, no. 11, pp. 6130–6140, Nov. 2015.

[2] W. Zhang, S. C. Wong, C. K. Tse, and Q. Chen, "Design for efficiency optimization and voltage controllability of series-series compensated inductive power transfer systems," *IEEE Trans. Power Electron.*, vol. 29, no. 1, pp. 191–200, Jan. 2014.

[3] K. Colak, E. Asa, M. Bojarski, D. Czarkowski, and O. C. Onar, "A novel phase-shift control of semibridgeless active rectifier for wireless power transfer," *IEEE Trans. Power Electron.*, vol. 30, no. 11, pp. 6288–6297, Nov. 2015.

[4] W. X. Zhong and S. Y. R. Hui, "Maximum energy efficiency tracking for wireless power transfer systems," *IEEE Trans. Power Electron.*, vol. 30, no. 7, pp. 4025–4034, Jul. 2015.

[5] T. Diekhans and R. W. D. Doncker, "A dual-side controlled inductive power transfer system optimized for large coupling factor variations and partial load," *IEEE Trans. Power Electron.*, vol. 30, no. 11, pp. 6320–6328, Nov. 2015.

[6] J. Huh, W. Y. Lee, S. Y. Choi, G. H. Cho, and C. T. Rim, "Frequency-domain circuit model and analysis of coupled magnetic resonance systems," *J. Power Electron.*, vol. 13, no. 2, pp. 275–286, Mar. 2013.

[7] C. K. Lee, W. X. Zhong, and S. Y. R. Hui, "Effects of magnetic coupling of nonadjacent resonators on wireless power domino-resonator systems," *IEEE Trans. Power Electron.*, vol. 27, no. 4, pp. 1905–1916, Apr. 2012.

[8] W. Zhong, C. K. Lee, and S. Y. R. Hui, "General analysis on the use of Tesla's resonators in domino forms for wireless power transfer," *IEEE Trans. Ind. Electron.*, vol. 60, no. 1, pp. 261–270, Jan. 2013.

[9] M. Kiani and M. Ghovanloo, "A figure-of-merit for designing high-performance inductive power transmission links," *IEEE Trans. Ind. Electron*., vol. 60, no. 11, pp. 5292–5305, Nov. 2013.

[10] F. Zhang, S. A. Hackworth, W. Fu, C. Li, Z. Mao, and M. Sun, "Relay effect of wireless power transfer using strongly coupled magnetic resonances," *IEEE Trans. Magn.*, vol. 47, no. 5, pp. 1478–1481, May 2011.

[11] D. J. Ahn and S. C. Hong, "A study on magnetic field repeater in wireless power transfer," *IEEE Trans. Ind. Electron.*, vol. 60, no. 1, pp. 360–371, Jan. 2013.

[12] S. A. Mirbozorgi, H. Bahrami, M. Sawan, and B. Gosselin, "A smart multicoil inductively coupled array for wireless power transmission," *IEEE Trans. Ind. Electron*., vol. 61, no. 11, pp. 6061–6070, Nov. 2014.

[13] R. Johari, F. V. Krogmeier, and D. J. Love, "Analysis and practical considerations in implementing multiple transmitters for wireless power transfer via coupled magnetic resonance," *IEEE Trans. Ind. Electron*., vol. 61, no. 4, pp. 1774–1783, Apr. 2014.

[14] S. C. Moon, B. C. Kim, S. Y. Cho, C. H. Ahn, and G. W. Moon, "Analysis and design of a wireless power transfer system with an intermediate coil for high efficiency," *IEEE Trans. Ind. Electron*., vol. 61, no. 11, pp. 5861–5870, Nov. 2014.

[15] W. X. Zhong, C. Zhang, X. Liu, and S. Y. R. Hui, "A methodology for making a three-coil wireless power transfer system more energy efficient than an two-coil counterpart for extended transfer distance," *IEEE Trans. Power Electron.*, vol. 30, no. 2, pp. 933–942, Feb. 2015.

[16] C. S. Wang, O. H. Stielau, and G. A. Covic, "Design considerations for a contactless electric vehicle battery charger," *IEEE Trans. Ind. Electron.*, vol. 52, no. 5, pp. 1308–1314, Oct. 2005.

[17] J. Sallan, J. L. Villa, A. Llombart, and J. F. Sanz, "Optimal design of ICPT systems applied to electric vehicle battery charge," *IEEE Trans. Ind. Electron.*, vol. 56, no. 6, pp. 2140–2149, Jun. 2009.

[18] R. Jegadeesan and Y. X. Guo, "Topology selection and efficiency improvement of inductive power links," *IEEE Trans. Antennas Propag.*, vol. 60, no. 10, pp. 4846–4854, Oct. 2012.

[19] C. S. Wang, G. A. Covic, and O. H. Stielau, "Power transfer capability and bifurcation phenomena of loosely coupled inductive power transfer systems," *IEEE Trans. Ind. Electron.*, vol. 51, no. 1, pp. 148–157, Jan. 2004.

[20] H. S. Choi, "Half-bridge LLC resonant converter design using FSFR-series Fairchild power switch," *Fairchild Semiconductor*, San Jose, CA, USA, Appl. Note AN-4151, 2007.

[21] J. Wang, J. Li, S. L. Ho, W. Y. Chau, W. K. Lee, W. N. Fu, Y. Li, H. Yu, and M. Sun, "Study and experimental verification of a rectangular printed-circuit-board wireless transfer system for low power devices," *IEEE Trans. Magn.*, vol. 48, no. 11, pp. 3013–3016, Nov. 2012.

[22] K. Fotopoulou and B. W. Flynn, "Wireless power transfer in loosely coupled link: Coil misalignment model," *IEEE Trans. Magn.*, vol. 47, no. 2, pp. 416–430, Feb. 2011.

[23] J. Wang, J. Li, S. L. Ho, W. N. Fu, Y. Li, H. Yu, and M. Sun, "Lateral and angular misalignments analysis of a new PCB circular spiral resonant wireless charger," *IEEE Trans. Magn.*, vol. 48, no. 11, pp. 4522–4525, Nov. 2012.

[24] A. K. RamRakhyani and G. Lazzi, "Multicoil telemetry system for compensation of coil misalignment effects in implantable systems," *IEEE Antennas Wireless Propag. Lett.*, vol. 11, no. 1, pp. 1675–1678, Jan. 2012.

[25] S. Aldhaher, P. C. K. Luk, and J. F. Whidborne, "Electronic tuning of misaligned coils in wireless power transfer systems," *IEEE Trans. Power Electron.*, vol. 29, no. 11, pp. 5975–5982, Nov. 2014.

[26] J. P. W. Chow, N. Chen, H. S. H. Chung, and L. L. H. Chan, "An investigation into the use of orthogonal winding in loosely coupled link for improving power transfer efficiency under coil misalignment," *IEEE Trans. Power Electron.*, vol. 30, no. 10, pp. 5632–5649, Oct. 2015.

[27] J. P. C. Smeets, T. T. Overboom, J. W. Jansen, and E. A. Lomonova, "Comparison of position-independent contactless energy transfer systems," *IEEE Trans. Power Electron.*, vol. 28, no. 4, pp. 2059–2067, Apr. 2013.

[28] H. Wu, G. Covic, J. Boys, and D. Robertson, "A series-tuned inductive-power-transfer pickup with a controllable AC-voltage output," *IEEE Trans. Power Electron.*, vol. 26, no. 1, pp. 98–109, Jan. 2011.

[29] X. Dai, Y. Zou, and Y. Sun, "Uncertainty modeling and robust control for LCL resonant inductive power transfer system," *J. Power Electron.*, vol. 13, no. 5, pp. 814–828, May 2013.

[30] B. Esteban, M. S. Ahmed, and N. C. Kar, "A Comparative study of power supply architectures in wireless EV charging systems," *IEEE Trans. Power Electron.*, vol. 30, no. 11, pp. 6408–6422, Nov. 2015.

[31] W. Zhang, J. C. White, A. M. Abraham, and C. C. Mi, "Loosely coupled transformer structure and interoperability study for EV wireless charging systems," *IEEE Trans. Power Electron.*, vol. 30, no. 11, pp. 6356–6367, Nov. 2015.

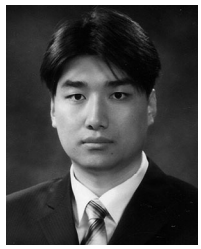

SangCheol Moon (S'10–M'15) was born in Jeju Island, Korea, in 1979. He received the B.S. degree in electrical engineering from Ajou University, Suwon, Korea, in 2005, and the M.S. and Ph.D. degrees in electrical engineering from the Korea Advanced Institute of Science and Technology, Daejeon, Korea, in 2007 and 2014, respectively.

He was a Visiting Student of Colorado Power Electronics Center, University of Colorado, in 2014.

He is currently a Staff Application Engineer in Fairchild Semiconductor, Bucheon, Korea, since 2007. His research interests include power electronics including analysis, modeling, control method, design of high-performance power converters, power factor correction, LEDs, and wireless power transfer systems.

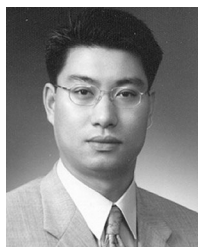

Gun-Woo Moon (S'92–M'00) received the M.S. and Ph.D. degrees in electrical engineering from the Korea Advanced Institute of Science and Technology (KAIST), Daejeon, Korea, in 1992 and 1996, respectively.

He is currently a Professor in the Department of Electrical Engineering, KAIST. His research interests include modeling, design and control of power converters, soft-switching power converters, resonant inverters, distributed power systems, power-factor correction, electric drive systems, driver circuits of plasma display panels, and flexible ac transmission systems.

Dr. Moon is a Member of the Korean Institute of Power Electronics, Korean Institute of Electrical Engineers, Korea Institute of Telematics and Electronics, Korea Institute of Illumination Electronics and Industrial Equipment, and Society for Information Display.